2024 IEEE/RSJ International Conference on Intelligent Robots and Systems (IROS)
October 14-18, 2024. Abu Dhabi, UAE

Design of a Pneumatically Driven 3D-Printed Under-Actuated Soft Robot with Programmable Stiffness

Zaid Mustafa[†] and Melih Türkseven[‡]

***Abstract*— Soft robotic technologies are laying the foundations for a wide range of applications involving manipulation, gripping, and locomotion. In particular, soft pneumatic actuators have been very popular for their high power-to-weight ratio and ability to yield significantly large motions. However, these actuators are usually limited in delivering reconfigurable deformation, limiting their versatility. A recent direction to rectify this limitation is to couple pneumatic actuation with active materials. Proof-of-the-concept designs has been developed to demonstrate that the actuator's deformation characteristics could be configured by selectively softening structural elements in an ON-OFF manner. In this paper, following this idea, we propose a novel soft pneumatic actuator coupled with stiffness programmable polylactic acid (PLA) elements. The proposed design is based on heating wires embedded in the PLA elements. Changes in the elastic properties of PLA near the glass transition temperature (T_g) coupled with pneumatic actuation are exploited to activate the actuator's variable stiffness features. This study shows that the stiffness of 3D-printed elements made of PLA can be tuned by means of temperature controlled heaters. The proposed actuator is able to extend by 19.5% of its original length and produce 15° angular deformation. We demonstrate the actuator's ability to perform different reconfigurable orientations based on different temperature and pressure inputs. The proposed idea could be considered as an actuation unit that can deliver complex deformations when configured in multitudes.**

I. INTRODUCTION

The interest in versatile soft robotic systems that offer adaptability to dynamic and complex situations has been motivating the demand for robot designs with reconfigurable deformation characteristics. Conventionally, these demands have been met through hyper-redundant designs, incorporating multiple serial segments, each with its independent actuator [1]. Although effective, such mechatronic designs tend to exhibit bulkiness and complexity [2]. Alternatively, recent applications focused on leveraging active materials for their potential to yield more compact solutions [3]. A promising approach in this direction is to utilize soft active materials to enable reprogrammable stiffness actuators [4][5]. This relatively new approach addresses both reconfigurability and compactness, enabling reconfigurable shape morphing in soft robots [6]. The technologies involved in these robotic systems include dielectric elastomers, thermofluidic polymers, and shape memory polymers [7] [8].

[†]Zaid Mustafa is with Faculty of Engineering and Natural Sciences, Sabanci University, 34956 Istanbul, Turkey zaid.mustafa@sabanciuniv.edu

[‡]Melih Türkseven is with Faculty of Engineering and Natural Sciences, Sabanci University, 34956 Istanbul, Turkey melih.turkseven@sabanciuniv.edu

Several designs have been proposed to show programmable deformability using stimulus responsive materials [9]. Systems that employ granular jamming could be considered as early examples [10]. While this approach yields a fast stiffness modulation, either it operates on the entire body or requires a vacuum source for every segment to be individually jammed. Shape-memory polymers (SMP) have been extensively used for reconfigurable deformation [11]. Alternatively, low melting point alloys (LMPA) were embedded to soft actuators to induce local stiffness modulation along the actuator body [12]. LMPA elements rapidly undergo a phase change when heated, inducing drastic drop in their stiffness. Reconfigurable deformation patterns could be attained when an array of such elements is embedded in a soft actuator such as a pneumatically driven actuator [13], or dielectric elastomer [14][15]. Although LMPAs exhibit drastic stiffness changes in a relatively fast manner, sealing these elements to impede leaking when LMPA is in liquid state is an essential part of the design. Both in the case of SMP and LMPA materials, the elements are used in ON-OFF configurations. They are either frozen, i.e. passive state in which they exhibit a high stiffness, or heated beyond their transition range, in which state they exhibit a significantly low stiffness [16]. Some limited robotic applications that exploit this concept have been presented [17][18].

This work introduces a novel pneumatically driven soft actuation unit that employs the reprogrammable stiffness concept to deliver reconfigurable deformation characteristics. In the presented design, the stiffness modulation is enabled via 3D-printed elements made of PLA. PLA is a ubiquitous thermoplastic polymer in 3D printing and can be easily used to fabricate elements in various shapes. Our study aims to realize easily fabricated, inexpensive and adept actuators with reconfigurable deformation patterns. Additionally, our study employs temperature control on these elements to explore the feasibility of stiffness tuning, as opposed to employing them in ON-OFF configurations as has been frequently done in the literature.

II. METHODS

The proposed soft actuator consist of three parts: 1) an inner inflatable elastomeric chamber, 2) a strain-limiting exoskeleton that encloses the inflatable chamber, and 3) heating elements attached to the exoskeleton.

A. Fabrication of the Actuator

The inflatable chamber is an elastomeric balloon that is made of a moldable silicone (*Dragon Skin 20, Smooth-On*).

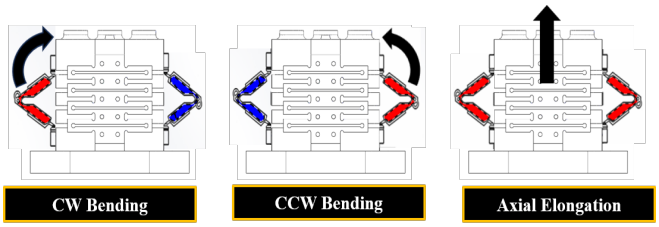

Fig. 1: Motion modes for the proposed actuator. The left configuration allows CW bending when only the left element is heated within T_g, the middle configuration allows CCW bending when only the right element is heated within T_g, and the right configuration allows axial elongation when both elements are heated to the same temperature within T_g. The inactive elements in the left and middle configurations are left at room temperature (i.e., 26 C°)

It has a diameter of 45 mm and a height of 54.5 mm. The thickness of the air chamber is 1.5 mm. This balloon is enclosed by a 3D-printed, cage-like structure. This part is printed using a flexible thermoplastic polyurethane (TPU) filament. It sets the deformation modes of the actuator to elongation and bending in a planar direction. The PLA element is an assembly of two parts: a V-shaped linkage made of PLA and connectors made of TPU to attach that linkage to the actuator, as shown in Fig. 2. The PLA part undergoes a transition from the glass phase to rubber phase when heated beyond its glass transition temperature. That is achieved via resistance wires with a diameter of 0.5 mm. The PLA heating elements' function is to induce a temperature-based asymmetry in the actuator's stiffness. This asymmetry is translated to a bending motion as the pressure inside the internal air chamber rises. When a PLA element on one segment of the actuator is heated, the entire segment bends towards the side with the less temperature; hence, the stiffer side. In the case that both PLA elements are heated to the same T_g, the actuator elongates axially.

B. Experimental Setup

The actuator's setup consists of electro-mechanical hardware that controls the temperature of the PLA elements and the pressure of the soft actuator, as outlined in Fig. 5. Heating wires embedded to the PLA elements are driven by current drivers via PWM (PCA9685). The temperature of these elements was controlled based on the feedback obtained by K-type thermocouples, which are also embedded to the elements. Temperature measurements were acquired using Labjack T7 data-acquisition card. A set of two solenoid valves (EnfieldTech) were utilized to inflate/deflate the soft actuator. The valves were operated via a DAC module connected to a microcontroller (STM32F4). The pressure was measured with an analog sensor connected to the Labjack T7 acquisition card. All of these equipment were operated with a single board computer (Raspberry PI4).

Additionally, the deformation of the actuator were monitored with an optical motion tracking camera (OptiTrack

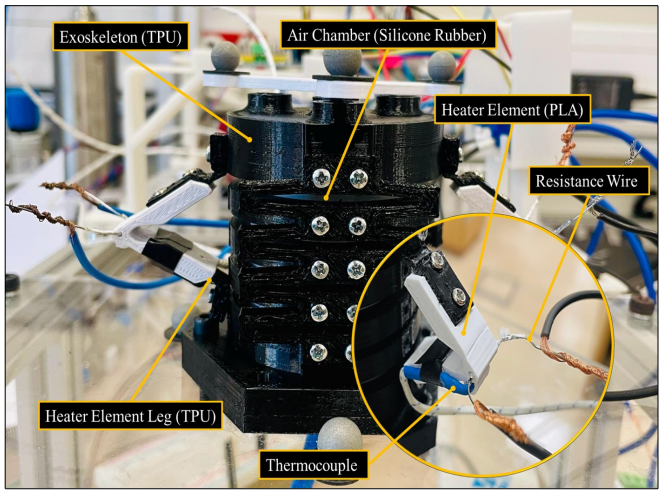

Fig. 2: 3D-printed design structure for a single segment soft actuator

v120:Trio) that was located above the actuator to get the position of a total of six markers at 120 Hz.

C. Kinematic Model of the Actuator

The proposed actuator can be considered as an elongating cylinder constrained by PLA elements acting as tendons [19]. Therefore, the constant-curvature model is employed to model the actuator's kinematics. This model assumes the entire backbone of the robot to have a uniform curvature along its length [20]. Figure 3 presents the measured marker positions and their relation to the calculated deformation variables of the constant-curvature model: the planar bending angle, θ, and the length of the central backbone of the actuator, l. Three markers were located at the base of the actuator ($\mathbf{p_1}, \mathbf{p_2}$, and $\mathbf{p_3}$ in Fig. 3) and another three at the tip ($\mathbf{p_4}, \mathbf{p_5}$, and $\mathbf{p_6}$ in Fig. 3). The marker positions were utilized to calculate the bending angle, θ, as follows:

$$\theta = \arccos\left(\frac{\mathbf{n}_b \cdot \mathbf{n}_t}{\|\mathbf{n}_b\| \cdot \|\mathbf{n}_t\|}\right) \tag{1}$$

where $\mathbf{n}_b$ and $\mathbf{n}_t$ are the normals of the actuator's base and tip plane, respectively. The normal direction of the tip plane can be calculated by computing the vectors $\mathbf{v_1} = \mathbf{p_5} - \mathbf{p_4}$ and $\mathbf{v_2} = \mathbf{p_6} - \mathbf{p_4}$, and then taking the cross product $\mathbf{v}_1 \times \mathbf{v}_2$. Similarly, $\mathbf{n_b}$ can be obtained via the markers at the base plane.

To compute the circular arc length l connecting the actuator's base and tip we must determine the centroid point of the base and tip planes as well the radius r of the arc. The former is simply $\mathbf{m_b} = \frac{\mathbf{1}}{\mathbf{3}}(\mathbf{p_1} + \mathbf{p_2} + \mathbf{p_3}) = (x_b, y_b, z_b)$ for the base plane and $\mathbf{m_t} = \frac{\mathbf{1}}{\mathbf{3}}(\mathbf{p_4} + \mathbf{p_5} + \mathbf{p_6}) = (x_t, y_t, z_t)$ for the tip plane. The radius r may then be computed by the following relation

$$r = \frac{c}{2sin(\frac{\theta}{2})} \tag{2}$$

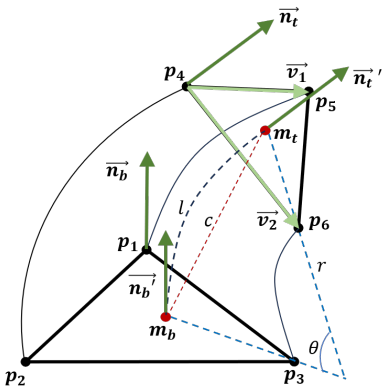

Fig. 3: Geometrical representation of the parameters describing the constant-curvature model used to quantify the bending and elongation of the proposed soft actuator

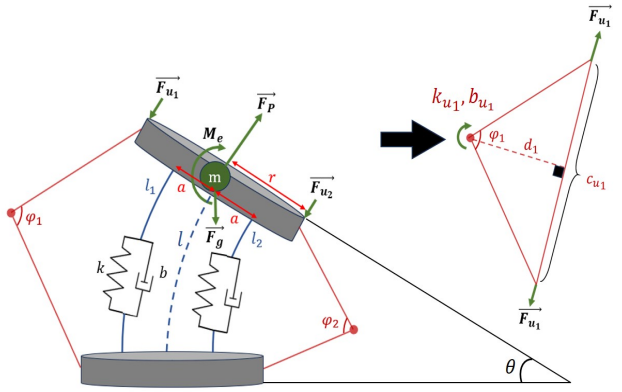

Fig. 4: Free-body diagram of actuator and its geometric modelling as a mass-spring-damper system

where c is the Euclidean distance

$$c = \sqrt{\sum_{i=1}^{3}(m_{t_i} - m_{b_i})^2} \tag{3}$$

denoting the chord length joining the actuator's base and tip points from Fig. 3. The arc length l is then given by

$$l = 2\pi r \frac{\theta}{360^\circ} \tag{4}$$

D. Quasi-static Mechanical Model of the Actuator

As shown in Fig. 4, the actuator can be respresented as a spring-mass-damper system under the influence of the following components: (i) The elasticity of the exoskeleton, which can be considered as a set of spring-damper couples, (ii) the PLA elements on either sides of exoskeleton to act as a two-link (single joint) mechanism with a torsional spring-damper at each joint. The weight of tip cap is denoted by the point mass *m* in Fig. 4. The gravitational force due to the tip cap, $\mathbf{F_g}$, and the associated inertial effects are neglected in our analysis due the limited rate of change of deformation and the insignificance of the tip weight in relation to the forces related to the internal pressure and the stifness of the actuator. The resulting quasi-static model of the system can be described as follows:

$$\mathbf{F_{u_1}} + \mathbf{F_{u_2}} = \mathbf{F_p} \tag{5}$$

$$\mathbf{M_e} - r\mathbf{F_p} + 2r\mathbf{F_{u_2}} = 0 \tag{6}$$

where $\mathbf{F_{u_1}}$ and $\mathbf{F_{u_2}}$ denote the forces acting on left and right PLA elements, respectively. The force $\mathbf{F_p} = \mathbf{P}.\mathbf{A}$ is due to the pressure pulse signal P exerted on the area A of the inner walls of the actuator's tip.

In equation (6), $\mathbf{M_e}$ is the bending moment generated by the actuator's exoskeleton made of TPU. The exoskeleton's innate stiffness is caused by the rhombus-patterned structures shown in Fig. 2. These rhombus-patterned structures can be approximated by spring-damper couples connected on each side of the central backbone, as shown in Fig. 3. In addition, both the exoskeleton structure and the inner balloon exhibits a bending stiffness that can be represented by a torsional stiffness coefficient, k_b. The rhombus-patterned structures' spring stiffness constant k, damping constant b, and the actuator's rotational stiffness constant k_b are related to M_e as follows:

$$M_e = (k\Delta l_1 + b\Delta \dot{l_1})(r+a) + (k\Delta l_2 + b\Delta \dot{l_2})(r-a) + k_b\theta \tag{7}$$

where $\Delta l_{1,2}$ represents the deformation of the rhombus-patterned structures on each side.

The forces F_{u_1} and F_{u_2} describe the tension applied by each PLA element, which can be modeled as a function of the extension in the element's joint, $\phi_{1,2}$. Assuming the joints of the PLA units act as spring-damper systems. the following models can be utilized to obtain the forces applied by the elements to the exoskeleton of the actuator:

$$F_{u_1} d_1 = k_{u_1}\varphi_1 + b_{u_1}\dot{\varphi_1} \tag{8}$$

$$F_{u_2} d_2 = k_{u_2}\varphi_2 + b_{u_2}\dot{\varphi_2} \tag{9}$$

where the moments are written in terms of the angle φ inscribed by the legs of the PLA element in Fig. 4. Note that the moment arm of the PLA element, d_1 and d_2, changes significantly as the actuator deforms.

In this study, the parameters of the described mechanical models were experimentally obtained. The first experiment is focused towards identifying the stiffness and damping coefficients given in (7). The exoskeleton is constrained with an unactuated (high elasticity) PLA element on one side, while the other side remained unconstrained. The actuator is then deformed by applying an internal pressure of 0.6 bar. As there is only one PLA element in this configuration, M_e could be considered as the moment applied by the internal pressure. All of the kinematic variables of deformation could be obtained using the measured θ and l and basic geometric relationships. The parameters of interest were then acquired via applying least-squares approximation on (7). Following the identification of the exoskeleton model, a new set of experiments were conducted. This time both PLA elements were attached, while only one of them was heated to select

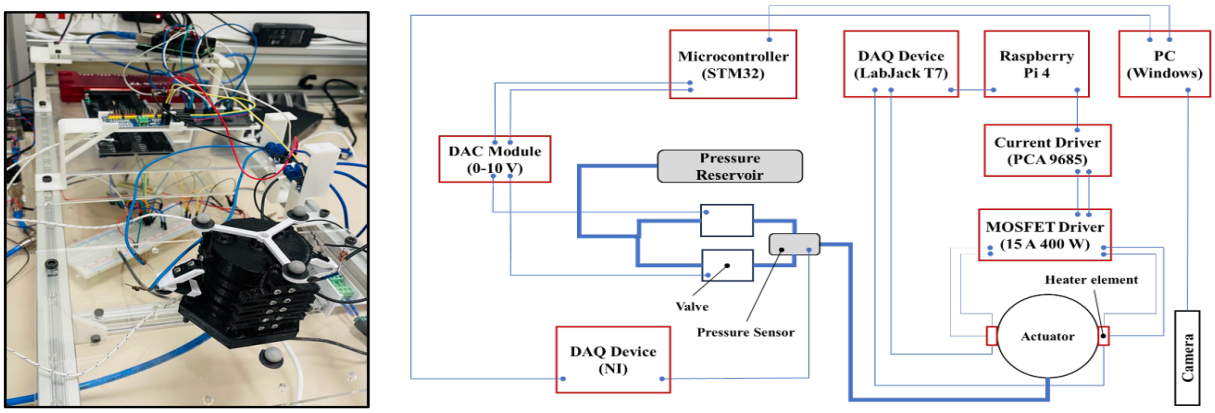

Fig. 5: Experimental setup (left) and wiring diagram (right)

temperatures (50, 55, 60, 65, and 70 Celcius). For each temperature configuration, the actuator was inflated to an internal pressure of 0.4 bar, 0.5 bar and 0.6 bar and deflated back. The resulting deformation variations for each case were used to obtain the corresponding mechanical model parameters of the actuated (heated) PLA elements.

III. Results

Fig. 6* shows the normal vectors ($\vec{n_t'}$ in Fig. 3) of the actuator's tip plane as they evolve over different temperature and pressure conditions. The range of temperatures chosen spans the glass-transition temperature T_g over which the PLA heater elements were subjected. The pressure range was chosen such that it involves the maximum pressure (determined by a process of trial and error) that does not compromise the structural integrity of the actuator's internal air chamber. In this case, the maximum pressure was $P_{gauge} = 0.6$ bar. The closer the vector group is to the plot's top right corner the greater the length deformation. Similarly, within each group, the greater the temperature of the PLA element, the closer the normal vector is to the top right corner. Fig. 7a and 7b represent the actuator's bending motion through the length change Δl and bending angle θ corresponding to temperatures between $50°C$ and $70°C$ for the cases where one or both heating elements are activated. Here, Fig. 7 shows the observed cases with most observed deformation. The trends clearly indicate that as the PLA element's temperature rises, its stiffness reduces considerably and, hence, the greater induced changes in length and inclination angles. According to Fig. 7a, the largest angular deformation of the actuator was observed to be $15°$ at a peak pressure of 0.6 bar.

In a similar fashion, we conducted an analysis for the case when both PLA elements of the soft actuator were heated simultaneously to temperatures within T_g (Fig. 7b). This time we anticipated the axial elongation of the actuator instead of bending motion. From Fig. 7b, we note that the maximum

*The negative axis values in Fig. 6 are used to represent correct normal vector orientations which are otherwise reversed due to the perspective of the optical camera frame.

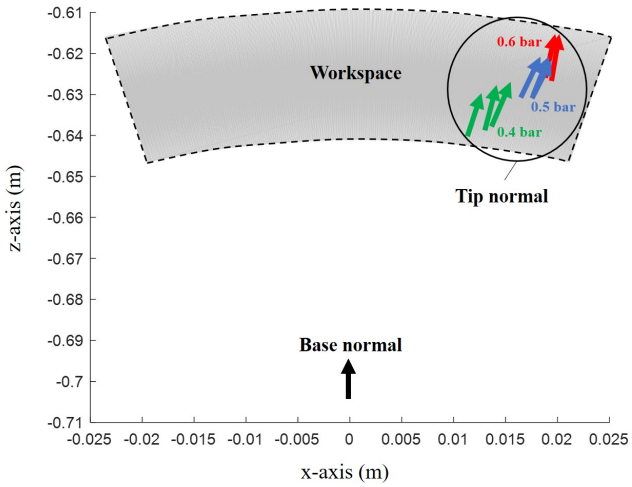

Fig. 6: Actuator tip plane normal vectors' workspace in relation to the base plane at different pressures.

axial elongation, 19.5%, occurred at $(70°C)$. Adding to the margin, one important factor distinguishing heating one vs both PLA elements in the proposed actuator was the additional motion constraint imposed by the rhombus-shaped structures on the middle rings of the exoskeleton (refer to Fig. 2). The minimum changes in Δl and θ occurred at around $50\ °C$. At these conditions, the PLA element exhibits higher stiffness as it operates near the low end of T_g. The nominal initial length of the actuator was measured to be 0.067 m as captured by the optical tracking camera.

Fig. 8 shows the PLA element's operating temperature evolving behavior when electrically heated at 2 watts. At the start, the PLA elements exhibit fast increase in temperature before slowing down at around the desired $70\ °C$, for example. A PID control law was implemented in Python to maintain the PLA element's temperature within a $\pm 1\ °C$. The element's cooling rate is relatively slower compared to the rising temperature time.

The stiffness and damping parameters described in equa-

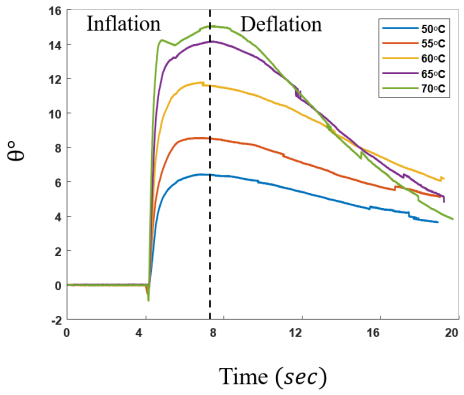

(a)

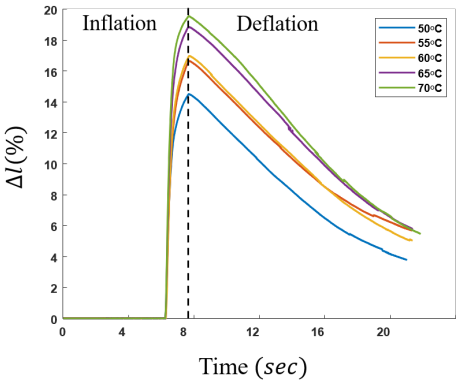

(b)

Fig. 7: Changes in lengths and bending angles as actuator deforms at different temperatures and activation modes. (a) reflects the angular deformations when one PLA element is heated while maintaining the other at room temperature, resulting in bending motion. The black dashed line roughly separates the inflation and deflation regions of the air chamber. In (b), both PLA elements are heated to the same temperature to invoke axial elongation.

tions (5) through (9) were obtained from experimental data using the method of least squares. The deformation of the actuator with the exoskeleton alone was utilized to determine the exoskeleton's elasticity parameters as $k = 2.23$ N/m, $k_b = 8.82$ Nm/rad, and $b = 88.28$ Ns/m with a coefficient of determination (R-squared) of 0.9428. Then, the parameters k_{u_1} and b_{u_1} (for the active element) for the PLA element's joints were identified using the pressure and deformation readings in the experiments shown in Fig. 6. The resulting model's arc length and bending angle estimations presented a satisfactory agreement with the experimental data (mean R^2: 0.832). We observed that beyond three cycles, thermal degradation leads to a 15% shape change and brittle behavior, leading to a slight increase in mismatch between model predictions and measured data. As expected, the PLA element's stiffness and damping properties exhibit a decreasing trend with increased temperature. The change rate of k_{u_1} and b_{u_1} with respect to temperature becomes progressively

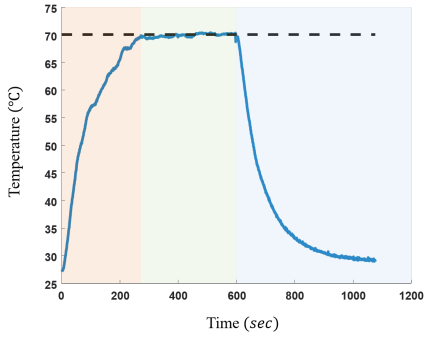

Fig. 8: PLA element's temperature rise (left region), controlled state (middle region), and temperature drop (right region) for an electrical power input of 2 watts.

Model Parameter	Temperature (C°)				
	50	55	60	65	70
k_{u_1} (Nm/rad)	0.0294	0.0287	0.0251	0.02094	0.02087
b_{u_1} (Nms/rad)	0.169	0.137	0.0807	0.0404	0.0355

TABLE I: Actuator estimated dynamic model parameters

slower towards the higher operating limit of T_g, indicating the approach of the PLA element's upper-limit elasticity.

IV. Discussion

The main efforts in this study revolve around designing, modelling, and validating a soft actuator based on the concept of heating 3D-printed elements to produce the effect of variable stiffness actuation. The proposed actuator can exercise two modes of motion: bending and axial elongation. As observed from the results in Fig. 6 and 7, the actuator is able to manifest linear and angular deformations based on different temperature and pressure inputs.

From Table I, we also numerically estimate the actuator's mechanical model parameters such as spring stiffness and damping coefficients at various temperatures. In addition to controlling the temperature at desired values, our proposed PLA elements also offer the opportunity for stiffness tuning. It is observed in Table I that stiffness can be modulated within a range of $15 - 20\ ^\circ C$, while our control accuracy is within $\pm 1\ ^\circ C$. This variability in stiffness introduces the potential for further optimizing the performance of our system. By precisely controlling the temperature of the elements within this narrow temperature range, we can potentially fine-tune the stiffness of the PLA element to generate predefined orientations. The proposed design offers the potential for a wide range of ideas including serially connecting a number of the aforementioned units to produce complex shapes. This can be achieved by, for example, increasing the number of exoskeleton rings (Fig. 2) and selectively heating specific elements to produce more complex poses. A multi-unit actuator may then be utilized for navigation purposes to reach behind obstacles, manipulate, or grasp objects where only a single valve and pressure control loop is required, contrary to other reported techniques where multiple valves

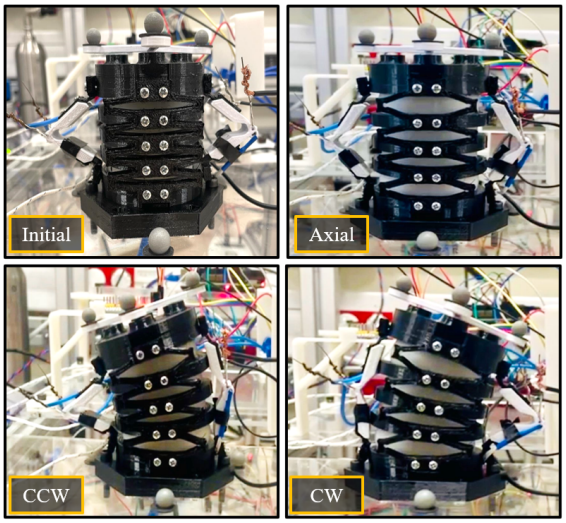

Fig. 9: An illustration of the soft actuator's different reconfigurable orientations. Initially, the actuator's orientation shows no bending or axial deformation (top left). Upward axial elongation (top right). CW bending motion (bottom right). CCW bending motion (bottom left).

and control loops can be necessary to achieve the same degrees of freedom.

Despite the working principle of the proposed actuator, our modeling analysis abandons considerations related to PLA's creep, hysteresis, viscoelastic behavior, and other time-dependent factors. Adopting models that take into account these factors can yield deformation predictions with higher accuracy, and wider workspace for the observed inclination angles and linear elongations. Furthermore, the element's heating cycle may be reduced with further design modifications, such as increasing the element's heated surface area and applying higher electrical power. Similarly, hastening the heating element's cooling rate is possible by the use of fans.

V. Conclusion

In this study, a pneumatically under-actuated single segment soft robot was proposed based on the concept of heating 3D-printed PLA elements to produce different reconfigurable orientations. The robot's variable stiffness PLA elements can be heated to reach PLA's glass-transition temperature upon which motion modes such as axial elongation, rightward, and leftward bending are achievable as can be seen from Fig. 9. The entire robot structure was fabricated using only 3D-printed PLA, TPU, and silicone rubber. Results in Fig. 6, Fig 7a, and 7b indicate that, under the experimentally induced pressure and temperature ranges, the actuator was able to achieve an inclination angle 15° in bending mode. In axial elongation mode, the actuator was able to achieve a maximum length increase of 19.5%. In future work, the proposed soft actuator design will be utilized in a multi-segment soft actuator to achieve more complex orientations. Additionally, a closed-loop control algorithm may be developed to permit precise reference tracking and manipulation.

References

[1] Z.-c. Du, G.-Y. Ouyang, J. Xue, and Y.-b. Yao, "A review on kinematic, workspace, trajectory planning and path planning of hyper-redundant manipulators," in *2020 10th Institute of Electrical and Electronics Engineers International Conference on Cyber Technology in Automation, Control, and Intelligent Systems (CYBER)*, pp. 444–449, IEEE, 2020.

[2] Z. Shen, F. Chen, X. Zhu, K.-T. Yong, and G. Gu, "Stimuli-responsive functional materials for soft robotics," *Journal of Materials Chemistry B*, vol. 8, no. 39, pp. 8972–8991, 2020.

[3] M. Schaffner, J. A. Faber, L. Pianegonda, P. A. Rühs, F. Coulter, and A. R. Studart, "3d printing of robotic soft actuators with programmable bioinspired architectures," *Nature communications*, vol. 9, no. 1, p. 878, 2018.

[4] X. Ke, J. Jang, Z. Chai, H. Yong, J. Zhu, H. Chen, C. F. Guo, H. Ding, and Z. Wu, "Stiffness preprogrammable soft bending pneumatic actuators for high-efficient, conformal operation," *Soft robotics*, vol. 9, no. 3, pp. 613–624, 2022.

[5] G. M. Whitesides, "Soft robotics," *Angewandte Chemie International Edition*, vol. 57, no. 16, pp. 4258–4273, 2018.

[6] S. Chen, Y. Cao, M. Sarparast, H. Yuan, L. Dong, X. Tan, and C. Cao, "Soft crawling robots: design, actuation, and locomotion," *Advanced Materials Technologies*, vol. 5, no. 2, p. 1900837, 2020.

[7] J. Zhang, Y. Wang, Y. Sun, S. Sun, Z. Xu, J. Li, J. Li, and X. Gong, "Multi-stimuli responsive soft actuator with locally controllable and programmable complex shape deformations," *ACS Applied Polymer Materials*, vol. 5, no. 8, pp. 6199–6211, 2023.

[8] A. O'Halloran, F. O'malley, and P. McHugh, "A review on dielectric elastomer actuators, technology, applications, and challenges," *Journal of Applied Physics*, vol. 104, no. 7, 2008.

[9] G. Decroly, A. Toncheva, L. Blanc, J.-M. Raquez, T. Lessinnes, A. Delchambre, and P. Lambert, "Programmable stimuli-responsive actuators for complex motions in soft robotics: Concept, design and challenges," in *Actuators*, vol. 9, p. 131, MDPI, 2020.

[10] J. Shintake, B. Schubert, S. Rosset, H. Shea, and D. Floreano, "Variable stiffness actuator for soft robotics using dielectric elastomer and low-melting-point alloy," in *2015 IEEE/RSJ International Conference on Intelligent Robots and Systems (IROS)*, pp. 1097–1102, IEEE, 2015.

[11] Q. Ze, X. Kuang, S. Wu, J. Wong, S. M. Montgomery, R. Zhang, J. M. Kovitz, F. Yang, H. J. Qi, and R. Zhao, "Magnetic shape memory polymers with integrated multifunctional shape manipulation," *Advanced Materials*, vol. 32, no. 4, p. 1906657, 2020.

[12] Y. Yang, Y. Chen, Y. Li, M. Z. Chen, and Y. Wei, "Bioinspired robotic fingers based on pneumatic actuator and 3d printing of smart material," *Soft robotics*, vol. 4, no. 2, pp. 147–162, 2017.

[13] S. Yoshida, Y. Morimoto, L. Zheng, H. Onoe, and S. Takeuchi, "Multipoint bending and shape retention of a pneumatic bending actuator by a variable stiffness endoskeleton," *Soft robotics*, vol. 5, no. 6, pp. 718–725, 2018.

[14] A. Jiang, G. Xynogalas, P. Dasgupta, K. Althoefer, and T. Nanayakkara, "Design of a variable stiffness flexible manipulator with composite granular jamming and membrane coupling," in *2012 IEEE/RSJ International Conference on Intelligent Robots and Systems*, pp. 2922–2927, IEEE, 2012.

[15] Y. Hao, J. Gao, Y. Lv, and J. Liu, "Low melting point alloys enabled stiffness tunable advanced materials," *Advanced Functional Materials*, vol. 32, no. 25, p. 2201942, 2022.

[16] L. Wang, Y. Yang, Y. Chen, C. Majidi, F. Iida, E. Askounis, and Q. Pei, "Controllable and reversible tuning of material rigidity for robot applications," *Materials Today*, vol. 21, no. 5, pp. 563–576, 2018.

[17] D. R. Yao, I. Kim, S. Yin, and W. Gao, "Multimodal soft robotic actuation and locomotion," *Advanced Materials*, p. 2308829, 2024.

[18] Y. Yang and Y. Chen, "Novel design and 3d printing of variable stiffness robotic fingers based on shape memory polymer," in *2016 6th IEEE International Conference on Biomedical Robotics and Biomechatronics (BioRob)*, pp. 195–200, IEEE, 2016.

[19] B. A. Jones and I. D. Walker, "Kinematics for multisection continuum robots," *IEEE Transactions on Robotics*, vol. 22, no. 1, pp. 43–55, 2006.

[20] R. J. Webster III and B. A. Jones, "Design and kinematic modeling of constant curvature continuum robots: A review," *The International Journal of Robotics Research*, vol. 29, no. 13, pp. 1661–1683, 2010.